



Cluster ions D_N^+ ejected from dense and ultra-dense deuterium by Coulomb explosions: Fragment rotation and D^+ backscattering from ultra-dense clusters in the surface phase

Patrik U. Andersson, Leif Holmlid*

Atmospheric Science, Department of Chemistry, University of Gothenburg, SE-412 96 Göteborg, Sweden

ARTICLE INFO

Article history:

Received 27 July 2011

Accepted 7 November 2011

Available online 16 November 2011

PACS:

67.63.Gh

61.46.–w

68.49.Sf

61.05.Np

Keywords:

Ultra-dense deuterium

Surface layer

Coulomb explosion

TOF-MS

Ion scattering

Cluster

ABSTRACT

The two forms of condensed atomic deuterium, dense deuterium $D(1)$ and ultra-dense deuterium $D(-1)$, can be studied by laser-induced Coulomb explosion time-of-flight mass spectrometry and neutral time-of-flight. In the present study pulsed laser intensity below $10^{14} \text{ W cm}^{-2}$ is used. Cluster ions D_N^+ from $D(1)$ are observed with $N = 3, 4, 12$ and 17 , thus not in close-packed forms. Clusters $D_N(1)$ are mainly in the form of chains of D_2 and D_3 groups, a shape derived from the $D(-1)$ material which $D(1)$ is spontaneously converted to. Only atomic ions D^+ with initial kinetic energy of hundreds of eV are observed from $D(-1)$. Half of these ions are ejected from the emitter surface, half of them penetrate into the ultra-dense $D(-1)$ layer on the emitter surface. This second half of the ions is reflected completely from the surface layer formed by ultra-dense $D(-1)$ strongly bonded clusters $D_3(-1)$ and $D_4(-1)$.

© 2011 Elsevier B.V. All rights reserved.

1. Introduction

Dense deuterium $D(1)$ [1–5] and ultra-dense deuterium $D(-1)$ [1,2,5–10] have been studied in our laboratory with laser-induced mass spectrometry (TOF-MS) of ions formed by characteristic Coulomb explosions (CE). Similar time-of-flight methods for neutral fragments have also been used. $D(1)$ and $D(-1)$ are two forms of the same material, which rapidly interconvert, with $D(1)$ being of the general Rydberg matter (RM) [11–14] type. They are the lowest energy state of RM with a small barrier towards inter-conversion [7,10]. Due to the extremely high density of $D(-1)$, of the order of 10^{29} cm^{-3} (140 kg cm^{-3}) it is believed to be very useful as target material for inertial confinement fusion (ICF) using intense pulsed lasers [1,2,6,7,9,15]. Recent results show fusion without ignition in this material [9]. The ultra-dense material is only formed by deuterons, making the fusion process $D + D$ attainable more easily. The main beneficial properties as fusion targets are the extremely high density and also the high-energy deuterons released in the

material by laser pulses [8]. The amount formed regularly in the laboratory is less than $1 \mu\text{g}$ [7] since this amount is enough to give ignition in a fusion reaction [16].

The catalytic process of forming ultra-dense deuterium $D(-1)$ starts from $D(\text{RM})$ at high excitation levels $D(3)$ and $D(4)$, falling down in energy to dense deuterium $D(1)$ which is spontaneously converted into ultra-dense deuterium $D(-1)$ [1,2,7]. The present study is concerned with the ion clusters which can be observed by laser initiated CE, and with the clusters which exist in the ultra-dense surface layer on the catalytic emitter. The excitation level is generally indicated as $D(l)$, where l is the angular momentum quantum number. This is the main quantum number describing the material. The basis for the description of $D(-1)$ is that this material is similar to an inverted form of $D(1)$, where the deuterons and the electrons have exchanged their roles. This is based on the general ideas of dense hydrogen materials by Ashcroft and other authors [17,18]. The reason for this inversion is probably the fact that the deuterons are bosons and thus do not resist the inversion to the ultra-dense material. In the case of protium, no separate ultra-dense form has been observed so far. The quantum mechanical basis for $D(-1)$ was recently discussed by Winterberg [16,19]. The $D(-1)$ material is expected to be both superfluid and

* Corresponding author. Tel.: +46 31 7869076.

E-mail address: holmlid@chem.gu.se (L. Holmlid).

superconductive at room temperature and is probably formed by exchange forces between the deuterons [16,19]. Only hydrogen isotope atoms are expected to give an ultra-dense material form, since the inner electrons prevent this inversion for all other atoms.

2. Theory

The main emphasis in the present study is on the material forms D(1) and D(-1) which constitute the lowest energy state of D(RM). They thus lack any excited state properties of general RM. They are stable for days at low pressure in the laboratory [7]. The conduction band electrons in D(1) are excited and delocalized as in general RM. Thus, the properties of D(1) are those of a condensed metallic phase, not of separate Rydberg species. The difference between RM and an ordinary metal is that the conduction electrons in an ordinary metal have orbital angular momentum $l=0$, while RM is characterized by $l \geq 1$. In RM, the potential for the conduction electrons is neither central due to their comparable distances to several ions, nor of the form $1/r$ [14]. This means that the only good quantum number is the orbital quantum number l (spin quantum numbers also exist). Since the principal quantum number for a free atom n does not exist, a condition $l < n$ does not exist either. To distinguish between the quantum numbers for free atoms and the condensed phase, the excitation level n_B (B for Bohr model) is introduced, numerically equal to the orbital electron angular momentum l . RM at excitation levels $n_B = 3-8$ is normally observed in the form of planar six-fold symmetric clusters with magic number $N=7, 19, 37, 61$ and 91 [14,20,21]. Many experimental methods have been used to characterize and study the processes that form Rydberg species and RM in desorption from the RM emitter materials, as well as the RM cluster phase directly. Rotational spectroscopy gives accurate information about planar RM cluster forms and bond distances at excitation levels $n_B = 4-8$, in good agreement with other experiments and theory [20,22].

Theoretical classical calculations with electron correlation taken into account [14] show that, even though the RM electrons are delocalized in the RM clusters, it is still possible to describe them as moving in stable circular orbits that are scaled by n_B^2 . Further, it was concluded that bonding may only exist when all the electrons have the same excitation level in the RM cluster: dephasing will otherwise take place. Thus each classically stable orbit determines the interionic bond length $d = 2.9n_B^2 a_0$, where a_0 is the Bohr radius. The approximate scale factor 2.9 was determined in quasi-classical stability calculations of RM clusters [14]. It was recently determined with high precision by rotational spectroscopy of RM clusters [22] and shown to vary slightly with cluster size N and excitation level n_B [20].

When a laser pulse passes through the dense materials D(1) and D(-1), the photons may excite (displace) one bonding electron between two adjacent atoms so that two ions become exposed to each other. A simple picture of the process proposed to take place in D(1) is shown in Fig. 1. In the case of D(-1), a similar process takes place but with the electrons initially only shielding the deuterons in each D₂ pair in the chain cluster. Coulomb repulsion makes the ions move apart rapidly, in <1 fs for D(-1). When the CE takes place, the ions fly apart with almost all their repulsion energy as kinetic energy release (KER) in the ionic fragments. Thus, it is possible to determine the initial repulsion energy between the ions by measuring the kinetic energy of the fragments at a distance from the actual explosion event. Then, the distance between the ions before the break-up i.e. the bond length is found directly from the Coulomb formula as

$$r = \frac{1}{4\pi\epsilon_0} \frac{e^2}{E_{\text{kin}}} \quad (1)$$

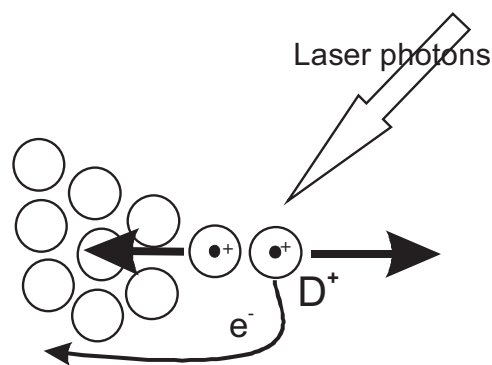


Fig. 1. Schematic drawing of a Coulomb explosion (CE) process in dense deuterium D(1). After removal of an electron by a laser pulse, two deuterons are exposed to each other.

where ϵ_0 is the vacuum permittivity, e the unit charge and E_{kin} the sum kinetic energy for the two fragments (KER) from the CE. The fraction of the KER that is observed on each fragment depends on the mass ratio of the fragments. The kinetic energy is determined most easily by measuring the time-of-flight (TOF) of the particles and converting this quantity to kinetic energy. This requires that the mass of the particle is known or can be inferred, which of course is simplified when working with just deuterium.

Dense deuterium D(1) is in most respects similar to H(1), which has been studied in several publications [4,23–25]. This means that the interatomic bonding distance d_1 derived from the observed KER of 9.4 eV is close to $2.9 \times 52.9 \text{ pm} \approx 153 \text{ pm}$ [24,25]. The geometry of the orbitals at $l=1$ is not strictly planar, giving various cluster forms. The H(1) ion and neutral clusters can be both planar, as for higher RM levels, and also close-packed 3D like tetrahedrons and octahedrons [4].

The internal form of the ultra-dense material D(-1) is not known very well. For example, the observed pairing of the electrons in the D(-1) clusters is not well understood, while the pairing of the deuterons probably is due to exchange forces [16,19]. It is likely that the deuterons rotate around the center of mass of the pair. This explains the transformation between D(-1) and D(1) as due to angular momentum conservation with a switch from orbital electron to orbital deuteron motion [5] as expected for an inverted material. The energy level of D(-1) is close to that of D(1), since the inter-conversion between these two forms is facile in the experiments. The observed general KER of 630 eV (varying with the detailed CE fragmentation process) gives a bond distance of $2.3 \pm 0.1 \text{ pm}$ [1,2,5]. This is close to the expected distance in an inverted material of $d_{-1} = (m_e/m_D)^{1/2} d_1$ equal to 2.5 pm [2,5].

3. Experimental

The apparatus and the methods used here have been described in several publications: see examples in refs. [24,26]. A few different constructions of the central emitter part giving the dense and ultra-dense hydrogen materials have been used, while the detector part in the UHV chamber is the same. The emitter is a sample of an industrial iron oxide catalyst doped with K (initially at 8 wt%) [27,28]. It is of the (now obsolete) styrene catalyst type Shell S-105, but several other similar catalysts work. The emitter is either mounted in a Ta foil holder with a flat surface area of $3 \times 10 \text{ mm}^2$ exposed to vacuum, or held in the opening of a heated tube for the gas feed. The Ta foil holder shown in Fig. 2 can be moved perpendicularly to the laser beam, and a voltage up to 500 V may be applied to the emitter in this construction. In the other construction, the emitter can be moved around the center of the chamber in all directions. The emitter is heated by an ac current through the Ta foil or through the gas feed tube to a temperature $<500 \text{ K}$. Deuterium gas ($>99.8\%$

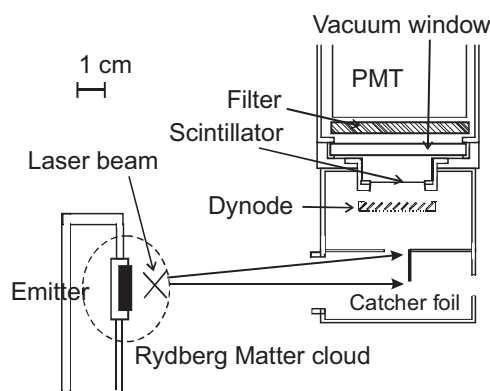


Fig. 2. Cut through detector shown sitting at 90° towards the laser beam which passes into the plane of the drawing. Fast particles hit the catcher foil, while ions are deflected and attracted towards the dynode by the dynode field extending in front of this foil.

D_2) is admitted at a pressure up to 3×10^{-5} mbar. A Nd:YAG laser with an energy of <200 mJ per each 5 ns long pulse at 10 Hz is used at 532 nm. The laser beam is focused with various lenses, mainly $f=50$ and 400 mm spherical lenses, at the center of the UHV chamber. The laser intensity in the beam waist varies between 10^{11} and 10^{14} W cm^{-2} as calculated for a Gaussian beam.

The detector is a dynode–scintillator–photomultiplier setup that is described in detail elsewhere [24] and shown in Fig. 2. The detector is here located at an angle of 90° or 45° from the incoming laser beam and measures the neutral TOF spectra or TOF-MS spectra (with a voltage applied to the emitter). Fast neutral particles are converted to ions at a catcher foil in the detector. The ions are accelerated towards a Cu–Be dynode held at -8.0 kV inside the detector. The total effective flight distance for the ions from the laser focus to the dynode is 113 mm while the neutral flight distance to the catcher foil is 101 mm, both distances directly measured and verified by internal calibration [3]. The photomultiplier (PMT) is Electron Tubes 9813B with single electron rise time of 2 ns and transit time of 46 ns, or Electron Tubes 9128 with single electron rise time of 2.5 ns and transit time of 30 ns. Blue glass filters in front of the PMT decrease the pulsed laser signal strongly. The signal from the PMT is collected by a multi-channel scaler (EG&G Ortec Turbo-MCS) with preamplifier or observed on a fast oscilloscope with signal averaging possibilities. The dwell time used here per channel in the MCS is 5 ns. Each MCS spectrum consists of a sum of the fragment signals from 250 or 500 laser shots.

4. Results

To simplify the presentation, the results are often shown in reduced (E-compensated) plots where all time scales are recalculated individually to compensate for the varying acceleration voltage. The multiplicative time scale factor in each spectrum is $(U_{\text{acc}}/500)^{1/2}$, with U_{acc} the emitter voltage in V. This means that with no KER, ions will appear at the same reduced TOF independent of the emitter voltage. This property is not caused by any special effects but is due to the general scaling properties of the electric field. With a substantial KER, the ions appear to shift to shorter TOF at lower emitter voltage in such plots due to their initial kinetic energy before acceleration in the TOF-MS. This means that a quantity that does not scale with the acceleration voltage is introduced in the equations for the ion motion. All TOF given in the text and the tables are measured from the first peak in the direct laser-induced photon peak in the spectra, i.e. the first peak in each spectrum at 45–50 ns time from the zero in the displayed spectrum. This 45–50 ns delay is due to the transit time in the PMT.

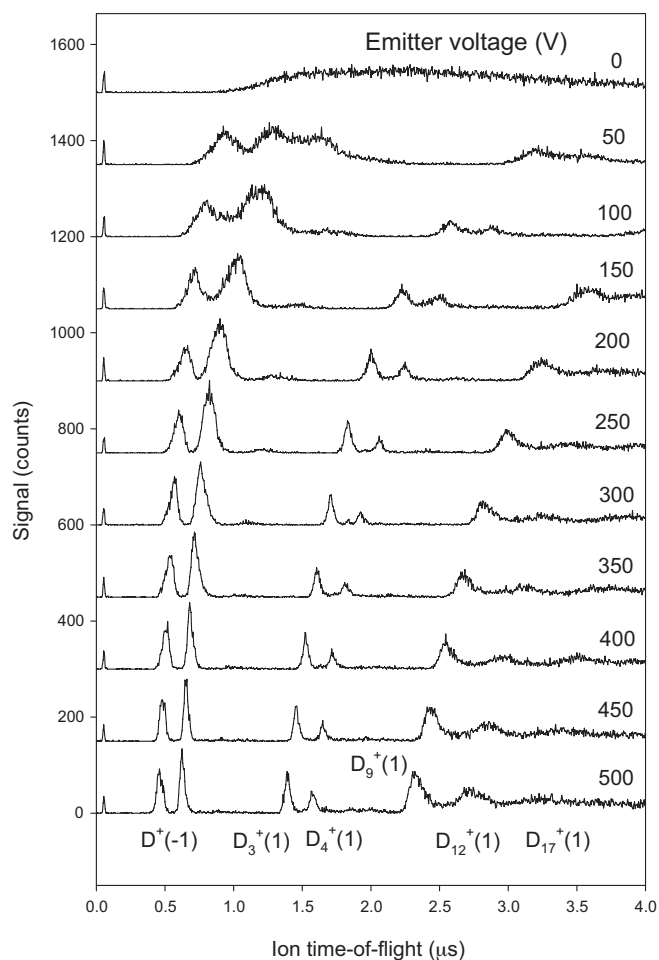


Fig. 3. Well resolved deuterium D(1) and D(–1) TOF-MS spectra with emitter (acceleration) voltage as parameter. Laser power 1.0 W at 10 Hz, D_2 gas admission, detector at 90° relative to the incoming laser beam. Spectra are displaced arbitrarily upwards to increase visibility. See Tables 1–3 for peak assignments and calculated peak positions.

4.1. Identification of D(–1)

In the TOF-MS experiments, the ion acceleration voltage (emitter voltage) is varied systematically. The TOF pattern varies with voltage, which shows that ions are indeed observed and not fast neutrals. Such experiments also give direct information on the KER of the individual ion types in the Coulomb explosions. An example with D^+ ions and D_N^+ cluster ions is shown in Fig. 3. An overview of the peaks observed at 500 V acceleration voltage is given in Table 1. An analysis is given in Table 2 for the D^+ ions from D(–1). The particles observed are described with similar spectra in other publications [1,2,5], but the conclusions are here improved and extended. Finally, the cluster ions from D(1) in Fig. 3 are for completeness analyzed in Table 3 but are described in detail in a later subsection.

In Fig. 3, the two closely spaced peaks at the shortest TOF are due to D^+ ions from D(–1). A protium ion H^+ starting with zero initial kinetic energy (zero KER) would have a TOF of 600 ns at 500 V acceleration voltage. There is no protium in the system in this case but only deuterium, and a D^+ ion accelerated from zero KER would have a TOF of 849 ns. In the figure, the first peak is at 395 ns and the first rise of signal is at 350 ns at 500 V acceleration voltage. Thus, it is proved that the peaks are due to ions D^+ with a considerable KER thus an initial kinetic energy from the formation process. In Table 2, these peaks are analyzed in detail. As can be seen there,

Table 1

Overview of assignments of the D(−1) and D(1) TOF-MS peaks in Fig. 3 for emitter voltage 500 V. The KER represented by (3+) is due to repulsion by two stationary charges.

TOF (ns)	eV/2u	Assignments	E_{kin} (eV) calc.	TOF (μs) observed (peak)	TOF (μs) calc.	Assignments (9.4 eV initial energy)
347 (start)	800	D ^{+(−1)} (3+) 2 ↔ 4	839	1.33	1.32	D ₃ ⁺ (1)
395	550	D ^{+(−1)} (see Table 2)	551	1.52	1.53	D ₄ ⁺ (1)
571	130	D ⁺ (550 eV) 2 → 6 refl.	138	2.25	2.29	D ₉ ⁺ (1)
825	0.7	D ⁺ from D ₂ gas	0	2.65 3.16	2.64 3.14	D ₁₂ ⁺ (1) D ₁₇ ⁺ (1)

Table 2

Assignments of the D(−1) TOF-MS peaks in Fig. 3. Column 3 gives the assignments for the kinetic energy E_{kin} in column 4, assuming a KER of 630 eV and a small cluster D₂ as absorbing part of the KER in rotation. Columns 5 and 6 give the observed and calculated values for the scattered second TOF-MS peak in the spectra, using the observed kinetic energy in column 2 for the impinging ion.

U_{acc} (V)	D ^{+(−1)} (eV/2u)	J(D ₂)	E_{kin} (eV/2u) calc.	D ^{+(−1)} (scatt) (eV/2u)	D ⁺ scattered off D ₃ –D ₄ (eV)
0	30 (peak) 130 (start)	12	19	–	–
50	145	11	113	60 and 24	36–52
100	180			42	45–65
150	210	10	198	55	53–76
200	240			68	60–86
250	280	9	277	73	70–101
300	320			98	80–115
350	355	8	348	115	89–128
400	430	7	411	120	108–155
450	450	6	465	120	113–162
500	550	4	551	130	138–198

the KER is large, as high as 550 eV in the fastest ion peak at 500 V acceleration potential. Observe that the ion in this case moves with 1050 eV inside the detector before acceleration by the dynode field. The only possible known process which may form ions with such high kinetic energy is a CE process acting at very short bond distances of the order of a few pm, much shorter than normal chemical bond distances.

In Table 2, the four first columns describe the first peak in Fig. 3. The assignment of the peaks is based on calculations using a bond distance of 2.3 pm [1,2,5] as the starting point for the CE processes, giving a sum of KER for both fragments of 630 eV. The second column gives the kinetic energy for a D⁺ ion arriving at the measured TOF, thus as eV/2u. The fourth column is the calculated energy for a D⁺ ion from the rotation excitation mechanism given in column 3. These results will be described further in the next subsection.

It is also interesting to study the TOF-MS spectra under identical conditions but with protium (ordinary hydrogen gas feed) instead of deuterium. When ordinary hydrogen gas H₂ is admitted in the chamber using a fresh catalytic emitter with no D adsorbed, the results in Fig. 4 are found. In this figure, the compensated type of plot is used to give an overview over all the TOF-MS spectra but the one with the emitter at zero potential which cannot be shown on this scale. The fastest ion is observed at 2000 ns using

an acceleration voltage of 500 V. This is much longer than for deuterium in Fig. 3 where the fastest ion peak was found at 395 ns, thus a factor of 5 shorter. Due to the mass difference, the ion peaks for H would be expected to arrive a factor of 1.4 faster than for D, thus the speed-up factor is 7 with this effect taken into account. This demonstrates very acutely that the material giving the deuterium spectra is entirely different from that giving the protium spectra. In the case of D, the material is a mixture of D(1) and D(−1) where the shape of D(1) is influenced strongly by the shape of D(−1). In the case of H, the material is H(1) which is the ground state of condensed atomic protium and which does not form an ultra-dense phase, at least not under the present conditions.

A full analysis of the results in Fig. 4 is given elsewhere [29]. It is enough here to point out that the spectrum shows large clusters of various sizes, from H₁₂⁺ up to H₇₀⁺. All these ions are from H(1) with a common KER of approximately 9.4 eV, which is verified by the degree of shifting of the TOF-MS peaks towards shorter reduced times at lower acceleration voltages. There is a clear tendency for clusters close to H_{7N}, with N = 2, 3, 4, 7 and 10 directly observed in Fig. 4. This agrees with planar RM clusters [14,20,22] H₇(1) stacked on top of each other. This form of cluster stacking was investigated theoretically in ref. [30] and was also concluded to exist from the nuclear spin-flip results in ref. [31].

Table 3

Measured and calculated TOF-MS peaks for small ion clusters from D(1) in Fig. 3. Initial kinetic energy of 9.4 eV is used in the calculations.

U_{acc} (V)	D ₃ ⁺ (1) (μs) observed (peak)	D ₃ ⁺ (1) (μs) calc.	D ₄ ⁺ (1) (μs) observed (peak)	D ₄ ⁺ (1) (μs) calc.	D ₉ ⁺ (1) (μs) observed (peak)	D ₉ ⁺ (1) (μs) calc.
50	3.13	3.32	3.54	3.83		
100	2.53	2.59	2.81	2.99	4.2	4.5
150	2.17	2.21	2.43	2.56	3.54	3.85
200	1.94	1.97	2.19	2.27	3.18	3.40
250	1.77	1.79	1.99	2.07	2.92	3.10
300	1.64	1.66	1.87	1.91	2.75	2.86
350	1.55	1.55	1.75	1.79	2.61	2.68
400	1.47	1.46	1.66	1.69	2.48	2.53
450	1.39	1.39	1.60	1.60	2.37	2.40
500	1.33	1.32	1.52	1.53	2.25	2.29

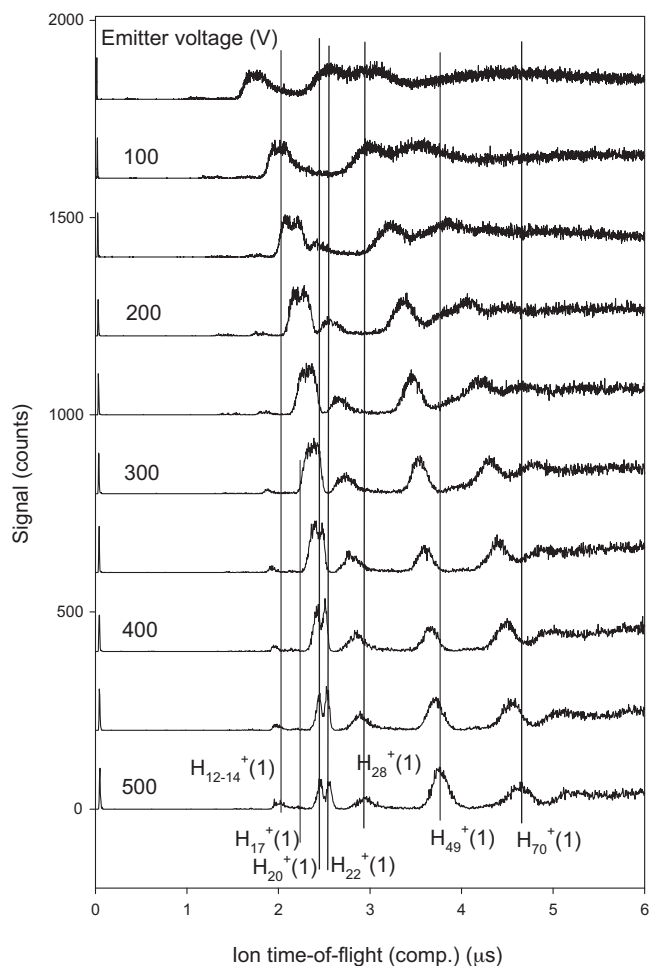


Fig. 4. Protium TOF-MS spectra from H(1) with emitter voltage as parameter. Laser power 1.6 W at 10 Hz, no gas admission, detector at 45°. The plots use reduced time axes, relative to the spectrum at 500 V emitter voltage. See further text. Spectra are displaced arbitrarily upwards to increase visibility.

4.2. KER of D^+ from $D(-1)$

For a more general discussion of the ions from $D(-1)$, the data in Fig. 3 are re-plotted in time compensated form in Fig. 5. The large KER for most ions is observed easily from the shifting in the compensated plots to shorter times at lower acceleration voltages. This point was shown numerically in Tables 2 and 3. The slowest possible D^+ ion (with KER 0 eV) will arrive after 849 ns (with 500 V emitter voltage), so all ions observed at longer times in Fig. 5 are cluster ions. A small peak is observed at 825 ns, which appears independent of the emitter voltage in the reduced plot. Thus, it has a very low KER, in this case <1 eV. It is unlikely that $D(3)$ or some other high excitation level is formed under the present conditions with relatively high electric field strength outside the emitter, and the most likely process giving D^+ with such a low KER is dissociation of D_2 molecules by collisions with the fast D^+ ions. The two strong peaks at 397 and 571 ns in Fig. 5 are due to D^+ ions with initial kinetic energy of 550 and 130 eV, respectively, thus from CE in the material $D(-1)$. An initial kinetic energy of 550 eV corresponds to repulsions $2 \leftrightarrow 10$, where the numbers are in mass units, thus $D^+ \leftrightarrow D_5^+$. The rise of the peak is at even higher energy, 800 eV. This corresponds to high-charge CE in a small cluster like $D^+ \leftrightarrow D_2^{2+}$. Such high-charge processes are described further below. An initial kinetic energy of 130 eV is too small for a simple repulsion, since even $2 \leftrightarrow 2$ gives 315 eV, and this means that these ions have been delayed by collisions. This point will be treated in a later subsection.

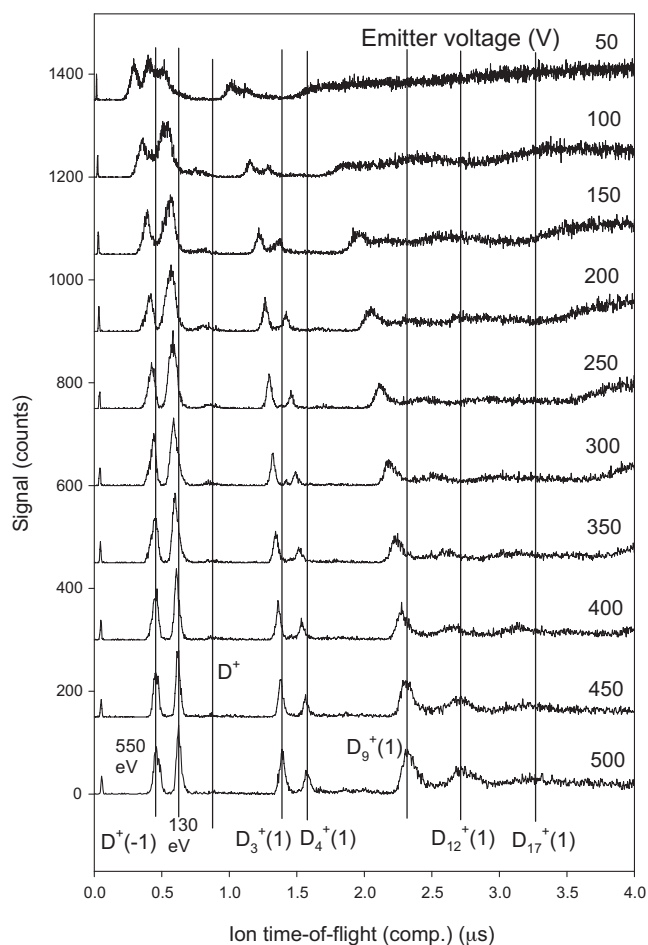


Fig. 5. Deuterium D(1) and D(-1) TOF-MS spectra with emitter (acceleration) voltage as parameter, same spectra as in Fig. 3. The plots use reduced time axes, relative to the spectrum at 500 V emitter voltage. See further text. Spectra are displaced arbitrarily upwards to increase visibility. See Tables 1–3 for peak assignments and calculated peak positions.

In Figs. 3 and 5 the process of ion formation from $D(-1)$, i.e. the first peak, is different from many other cases described [1,2,5]. This is found directly from the broad TOF distribution at zero acceleration voltage, where a long slow peak is observed, from 820 ns to 4 μ s. This is unusual, since normally very sharp peaks are observed also in neutral TOF [5]. Such sharp peaks can be accurately assigned to fragmentation processes in the $D(-1)$ clusters, similar to the assignments used here at 500 V emitter voltage. In the case in Figs. 3 and 5, another process dominates which gives broad peaks at zero acceleration, thus a very broad energy distribution of the neutral D atoms ejected, from 130 eV at the start to 10 eV in the tail of the peak. The process which gives the first ion peak in Figs. 3 and 5 also gives varying translational kinetic energy to the D^+ ions at higher voltage, between 550 and 145 eV as seen in Table 2. That the fragmentation process changes with the applied voltage is certainly possible since the size distribution can be influenced by the electric field strength, but here a different case is clearly found. A broad distribution at zero voltage normally indicates that large fragments are formed in the CE process from $D(-1)$ chain clusters [10]. Assuming a symmetric cleavage of chain clusters with KER of 630 eV shows that the distribution with zero voltage may be due to fragments from D at 820 ns to D_5 at the peak of 1.8 μ s and larger fragments for the tail. When a D_4 cluster is fragmented to $D^+ + D_3^+$, it is likely that the D_3^+ fragment receives a rotational energy in the CE process. Due to the short bond distance of 2.3 pm, even small rotational quantum numbers correspond to a substantial kinetic energy. Assuming a KER of

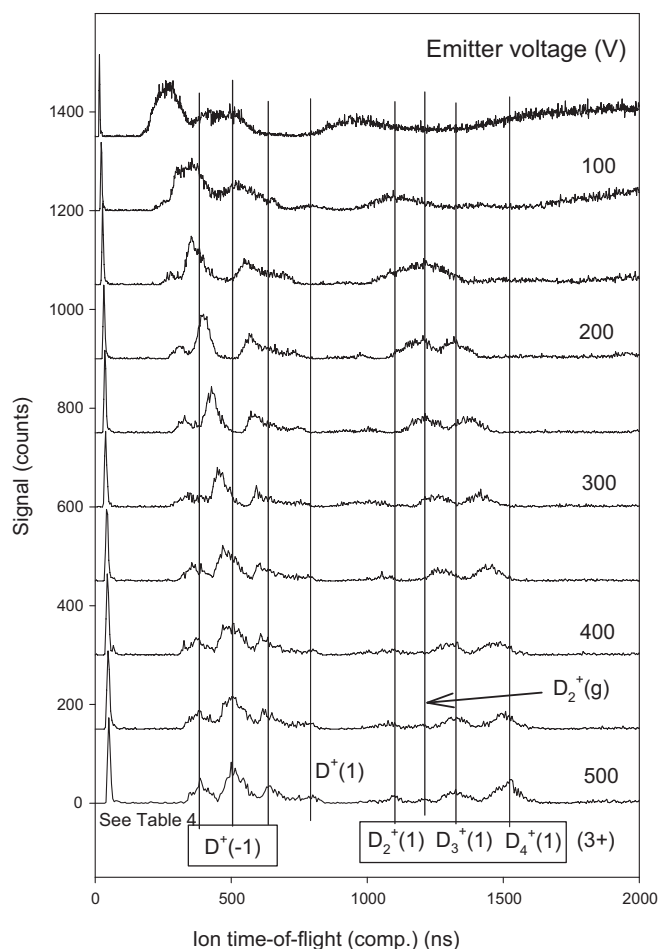


Fig. 6. High laser power D(1) and D(-1) TOF-MS spectra with emitter voltage as parameter. Laser power 1.6 W at 10 Hz, no gas admission, detector at 90°. The plots use reduced time axes, relative to the spectrum at 500 V emitter voltage. See further text. Spectra are displaced arbitrarily upwards to increase visibility. See Table 4 for peak assignments and calculated peak positions.

630 eV, the observed translational kinetic energies for the D^+ ions in Figs. 3 and 5 are described as due to rotational excitation in a D_2 fragment in Table 2. The D_2 fragment is the basic block in the chain clusters, and the rotation of a D_3^+ fragment is rather similar to the D_2 rotation. The agreement with the fragment rotation at $J=4-12$ is reasonable, in view of the complex fragmentation processes that are likely to take place. Thus, in this special case at least the agreement with a model giving large rotational energy to the stationary cluster fragment in the form of a chain cluster with D_2 beads agrees well with the experimental results. The redistribution of the KER to rotational degrees of freedom may be more complex, but it is quite clear that rotation is involved. It is likely that the electric field strength due to the applied acceleration voltage influences the size of the chain clusters, at low voltage allowing longer clusters which absorb more of the KER in rotation. More complex schemes for the distribution of the KER between translation and rotation are certainly possible but the present results show that an influence of the electric field strength on the fragmentation process is not sufficient to describe the energy in D^+ ion translation.

4.3. Ions $D^+(-1)$ from high-charge CE

The results in Fig. 5 are found with relatively low laser power. At higher laser power, the spectra change shape and the peaks become broader and also faster. An example is shown in Fig. 6, with detailed assignments in Table 4. The fastest peak there is observed at 333 ns,

with the initial rise of intensity at 286 ns. These TOF correspond to 900 eV and 1300 eV respectively. Such initial kinetic energies correspond to processes with repulsion of D^+ from two or three stationary charges, giving a KER up to 1260 and 1890 eV respectively. Such processes have been observed and described previously [8]. Very high initial kinetic energies up to 1300 eV are measured as shown. Most peaks in this type of spectrum with higher laser intensity are due to processes with KER of one small ion (the observed one) from two charges in the large stationary cluster. Thus, these processes involve three charges and will be identified as (3+) (which implies a change in nomenclature from the previous form (2+) indicating the number of repelling stationary charges in this type of process [1,5]). The process giving the first peak at 333 ns in Fig. 6 and Table 4 is a repulsion $D^+ \leftrightarrow D_3^{2+}$ which involves three charges. This is a fragmentation of a D_4 cluster with almost all electrons removed. Similar CE processes with all electrons removed in D_4 exist and are described below. The edge of this peak at 286 ns is located correctly for the asymptotic process $D^+ \leftrightarrow D_N^{2+}$ with N large. This process probably takes place at the end of a long chain cluster D_{2M} with M an integer. The other processes of the type (3+) are given in Table 4. It is clear that it is the higher laser intensity in this case which gives these high-charge CE processes.

4.4. Scattering of ions D^+ from D(-1) clusters

As shown in Fig. 3 and Table 2, the first TOF-MS peaks at 500 V are due to D^+ ions with high initial kinetic energy, at 550 and 130 eV respectively. The second peak is sharp and higher in intensity than the first peak. It cannot be due simply to a Coulomb explosion in a cluster of D(-1) like the first peak, since the initial kinetic energy of 130 eV is too low. It was suggested above that it is due to an ion scattering process: if D^+ with 550 eV collides with a D_3 cluster in a linear collision, 412 eV is transferred to the D_3 cluster and 138 eV is retained in the (backwards) D^+ motion. The first TOF peak is due to ions moving out from the emitter surface with 550 eV, and the second peak is thus due to ions initially moving with the same kinetic energy of 550 eV against the emitter surface, colliding with D_3 clusters and being reflected out from the emitter surface with 138 eV. This agrees well with the results in Fig. 3 as shown in Table 2, two last columns. In the last column, the first number is the energy after reflection against D_3 and the second after reflection from D_4 .

At low acceleration voltages in Table 2, D_3 clusters fit well as the scattering and reflecting objects. The reflection process is due to a D^+ ion. At large acceleration voltages, scattering from both D_3 and D_4 contributes to the scattered peak, since the observed peak is at energies intermediate between D_3 and D_4 scattering. However, another reason why the ion retains more energy at high acceleration voltage may be that the collisions are not exactly linear but non-central.

In the experiment with high laser intensity in Fig. 6, the first peak is at 900 eV and the broad second peak is centered at 330 eV as given in Table 4. This broad peak may correspond to collisions of 900 eV D^+ ions with D_4 clusters (giving 324 eV D^+). This peak may also have contributions from the CE process $2 \leftrightarrow 2$ giving D^+ with 315 eV (see Table 4). At the same time, reflections of D^+ with 315 eV colliding with D_4 in the surface layer gives an energy 113 eV, close to the observed peak energy of 100 eV. Thus, the three fastest peaks in Fig. 6 agree well with an ion scattering picture, with D^+ scattering against D_4 clusters.

In the well resolved experiment in Figs. 7 and 8, a clear structure of both the first and the second TOF peaks can be observed. The results for 500 V acceleration voltage will be studied in detail. The first peak with its three maxima is due to three slightly different CE processes as shown in the upper left-hand part of Table 5, with ions moving out from the surface. The equal number of ions with the same initial kinetic energies instead moving initially into the

Table 4
Assignments of the D(−1) and D(1) TOF-MS peaks in Fig. 6. The KER represented by (3+) is due to repulsion by two stationary charges. All data are for emitter voltage 500 V.

TOF (ns)	eV/2u	Assignments	E_{kin} (eV) calc.	TOF (μ s) observed (peak)	TOF (μ s) calc.	Assignments (KER 9.4 or 18 eV)
286 (start)	1300	D ⁺ (−1)(3+) 2 ↔ ∞	1260	0.754	0.763	D ⁺ (1)
333	900	D ⁺ (−1)(3+) 2 ↔ 6	944	1.05	1.08	D ₂ ⁺ (1)(3+)
460	330	D ⁺ (−1) 2 ↔ 2	315	1.17	1.16	D ₂ ⁺ (gas)
		D ⁺ (900 eV) 2 → 8 refl.	324	1.28	1.32	D ₃ ⁺ (1)(3+)
595	100	D ⁺ (315 eV) 2 → 8 refl.	113	1.48	1.53	D ₄ ⁺ (1)(3+)
754	11	D ⁺ (1)	9.4			

surface layer collide with D₃ clusters in this layer and are reflected, giving the second peak with its three maxima as shown in Table 5. It is observed that the intensities of the first and second peaks are almost equal, since half of the Coulomb explosions will eject ions against the surface, while half of the ions will leave the surface layer with no further collisions. (That no neutralization takes place for the ion scattering in the surface layer as in ISS or LEIS for other surfaces will be discussed below.) Thus, the second complex peak in the TOF-MS spectra provides an analysis of the clusters in the surface layer, showing that in this experiment the clusters existing in the surface layer are just D₃.

It is highly unlikely that these clusters D₃ and D₄ are of the type D(1), since the bond strength in D(1) is too small to make D(1) clusters behave as one body in the collision with D⁺ with kinetic energy 315–900 eV. This is in agreement with the results from ordinary ion scattering spectroscopy (LEIS, ISS) studies even on metal clusters on surfaces, where only ion-atom scattering is found due to the small bond energy relative to the impinging ion energy [32,33]. This means that the clusters D₃ and D₄ are of the form D(−1), with much stronger bonds than normal chemical bonds as expected due to the short bond distance. It is suggested that exchange forces between the deuterons are the cause of this strong bonding in D(−1) clusters [16,19]. The predicted bond energy between two deuterons is of the order of 700 eV. From studies of dimers D₂ [34] a value of at least 700 eV was found. This pairwise energy is probably sufficient to stabilize the clusters during impact of the D⁺ ions with energy 315–900 eV, even if the total bond energy in the clusters has not been calculated.

4.5. Ion clusters D_N⁺ from the D(1) material

At low laser power, the flux of cluster ions from the D(1) phase is relatively low and it is possible to identify the clusters by TOF-MS. A typical case is found in Fig. 3, with assignments in Tables 1 and 3.

Table 5
Assignments of the D(−1) and D(1) TOF-MS peaks in Figs. 7 and 8. All data are for emitter voltage 500 V. The KER represented by (3+) is due to repulsion by two stationary charges.

TOF (ns)	eV/2u	Assignments	E_{kin} (eV) calc.	TOF (μ s) observed (peak)	TOF (μ s) calc.	Assignments (KER 9.4 or 18 eV)
409	490	D ⁺ (−1) 2 ↔ 8	503	1.36	1.32	D ₃ ⁺ (1)
437	400	D ⁺ (−1) 2 ↔ 4	420	1.45	1.46	D ₄ ⁺ (1)(3+)
452	350	D ⁺ (−1) 2 ↔ 2	315	1.55	1.53	D ₄ ⁺ (1)
583	117	D ⁺ (490 eV) 2 → 6 refl.	123	2.36	2.29 2.41	D ₉ ⁺ (1) D ₁₀ ⁺ (1)
603	97	D ⁺ (400 eV) 2 → 6 refl.	100	2.73	2.75	D ₁₃ ⁺ (1)
613	90	D ⁺ (350 eV) 2 → 6 refl.	88	3.20	3.14 3.23	D ₁₇ ⁺ (1) D ₁₈ ⁺ (1)

The clusters clearly identified are D₃⁺, D₄⁺, D₉⁺ and D₁₂⁺, while the broad peak indicated D₁₇⁺ may contain a few different cluster forms. All these cluster ions have KER of approximately 9.4 eV and are thus from the condensed material of type D(1). In the case in Fig. 8 with lower laser power the assignments are given in Table 5. Clusters D₃⁺, D₄⁺ and D₁₃⁺ are verified, while less distinct peaks are found at the positions of D₉⁺, D₁₇⁺ and D₁₈⁺. These series of clusters have not been observed previously. For example, in ref. [4] the small ion clusters H_N⁺(1) were identified with a series with N=2, 4, 6 and 12 (N=3 also existed). These protium clusters are probably of the closed close-packed symmetric forms of dimer, tetrahedron, octahedron and (hollow) icosahedron. N=6 is not observed at all in the present experiments, which indicates other forms of bonding than the close-packed shapes observed for H(1) ions. The normal neutral planar cluster forms for high excitation levels in RM, with N=7, 19, 37 and 61 as identified by Coulomb explosions [21,35] and by rotational spectroscopy [20,22], are not observed here either. It appears rather that clusters with N=2 and 3 are some kind of basic building block. This may be extended to N=4 in the form of a tetrahedron which is formed by two pairs of D₂. The ion forms may certainly in general be different from the neutral cluster forms. The reason why the cluster forms for D(1) are different from those of H(1) will be discussed below: it is probably related to the rapid inter-conversion between the forms D(1) and D(−1) [7]. From the probable form of D(−1) clusters as chains of D₂ pairs shown in Fig. 9, it is proposed that also D(1) has a similar form due to this rapid inter-conversion.

The agreement between calculations and measurements is good. However, a trend is visible in the extensive Table 3 for the TOF at lower acceleration voltage, with the ions appearing earlier than predicted by the calculations. The cloud of matter around the emitter is larger at low field strengths, which means that the fragmentation and ionization will take place slightly further away from the emitter at low voltages. Including this effect in the calculations

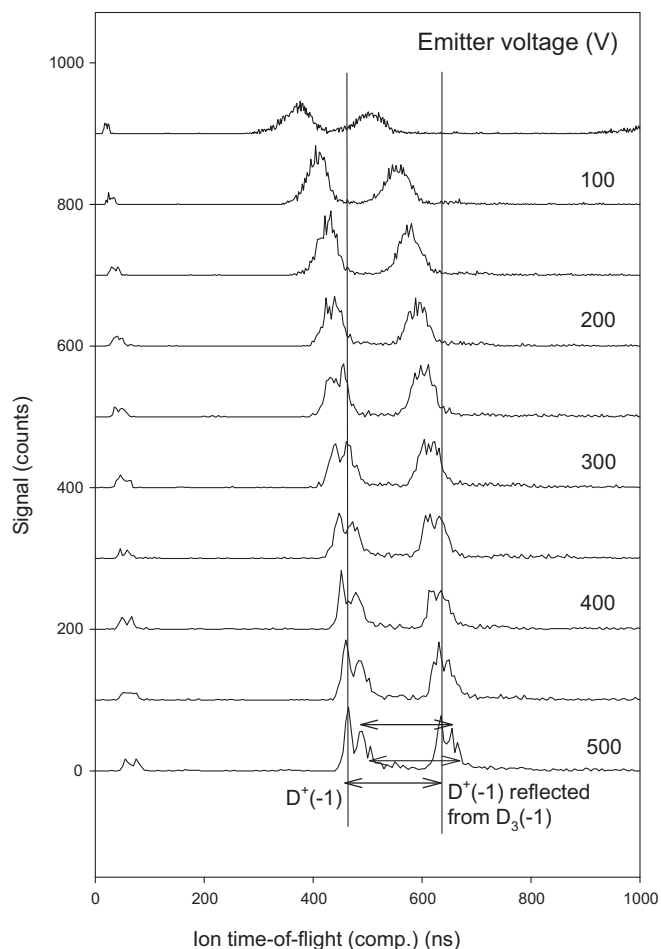


Fig. 7. Well resolved reflection peaks in deuterium $D(-1)$ TOF-MS spectra with emitter (acceleration) voltage as parameter. Laser power 0.27 W at 10 Hz , D_2 gas admission, detector at 90° . The plots use reduced time axes, relative to the spectrum at 500 V emitter voltage. See further text. Spectra are displaced arbitrarily upwards to increase visibility. See Table 5 for peak assignments and calculated peak positions.

gives better agreement, and this is the likely explanation for the shorter TOF at low voltages in Table 3.

With laser intensity of the order of 10^{11} W cm^{-2} , the fragmentation of the ion clusters is smaller. One example of a TOF-MS spectrum taken with a long flight path of 112 cm is shown in Fig. 10. The peak assignments are given in Table 6. Due to the long flight path, the somewhat non-ideal acceleration region close to the emitter has a very small influence on the TOF. This increases the precision in the TOF-MS in this case. The large cluster ions identified are primarily of the planar close-packed RM type like D_7^+ , D_{14}^+ (probably a dimer of D_7 as in the protium spectrum in Fig. 4) and D_{19}^+ . Thus, such planar clusters exist in $D(1)$ but they are not released as intact cluster ions at high laser intensities. $N=2, 6$ and 12 as in the close-packed series for $H(1)$ [4] are not observed. Other forms also exist in Fig. 10, and D_5^+ and D_9^+ may be of the chain-type of D_2 pairs suggested above, formed by central cleavage of longer chain clusters. In other experiments, a clear tendency for symmetric cleavage by the laser pulse like $D_{10}^{2+} \rightarrow 2 D_5^+$ exists (to be published). It is concluded that the bonding state of $D(1)$ here is very different from that of $H(1)$. The two first peaks in Fig. 10 due to $D(-1)$ show a distribution with initial kinetic energy of $630\text{--}315\text{ eV}$ in the first broad peak due to different fragmentation processes, and a sharp peak at 210 eV . This sharp peak corresponds to a reflection of D^+ with 585 eV initial kinetic energy in the surface layer against a cluster D_4 . The very sharp second peak indicates a time-focusing

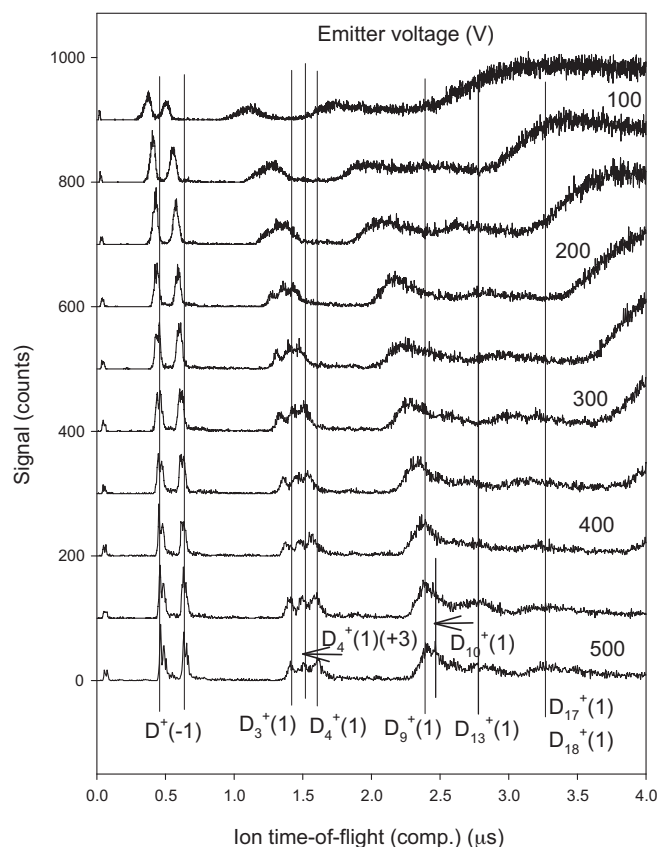


Fig. 8. Large cluster peaks in deuterium TOF-MS spectra with emitter (acceleration) voltage as parameter. Same data as in Fig. 7. See Table 5 for peak assignments and calculated peak positions.

due to this reflection in the surface layer since D^+ ions with higher initial kinetic energy will lose more kinetic energy than the ones with lower initial kinetic energy will do. Also in this case with lower laser intensity, the reflection of D^+ from clusters in $D(-1)$ is thus observed.

At high laser power, further features due to small ion clusters can be observed in the TOF-MS spectra. One illustrative example is given in Fig. 6, already partly described above. The peaks are assigned in the figure and in Table 4. D^+ ions are observed with high energies as well as at low energies. The peak at 900 eV corresponds to a repulsion $2 \leftrightarrow 6$ with two repelling charges in the heavier fragment of the cluster splitting apart. The peak at 754 ns is not due to $D(-1)$ but corresponds to $D^+(1)$, with initial kinetic energy of 9.4 eV . That the KER is low for this peak can be seen directly in Fig. 6, since the peak is shifting very little at lower acceleration

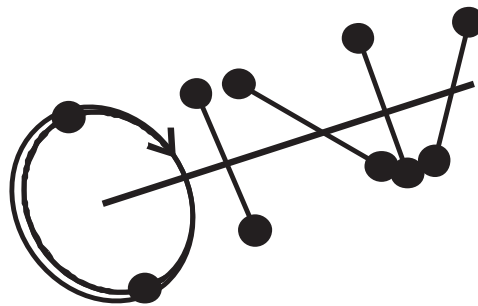


Fig. 9. Tentative shape of the chain clusters of superfluid ultra-dense deuterium $D(-1)$. The D_2 cluster “beads” are free to rotate around the axis given by the electron pairs.

Table 6
TOF-MS of D^+ and D_N^+ ions in Fig. 10 with interpretation. Long-path detector at 112 cm distance, emitter voltage 400 V. HM means half-maximum values.

Experiment (μ s)	Calculated (μ s)	Assignments	E_{kin} (eV) calc.
3.79–4.27 (HM)	3.79–4.26 (HM)	D^+	530–340 (HM)
4.69	4.71	D^+ (585 eV) $2 \rightarrow 8$ refl.	210
11.5	11.9	$D_4^+(1)$	9.4
13.6	13.3	$D_5^+(1)$	9.4
15.6	15.7	$D_7^+(1)$	9.4
18.1	17.8	$D_9^+(1)$	9.4
19.5	19.7	$D_{11}^+(1)$	9.4
22.5	22.2	$D_{14}^+(1)$	9.4
26.1	25.8	$D_{19}^+(1)$	9.4

voltages. The remaining peaks to the right in the figure are cluster peaks from $D(1)$. Most of them are due to repulsion from two charges, with the slowest one at 1.48 μ s. It is due to repulsion of D_4^+ from two stationary charges, giving an initial kinetic energy close to 18 eV (2×9.4 eV) [24]. The other peaks are similar but due to D_2^+ and D_3^+ . The smallest peak in this range, at 1.17 μ s has a different origin, since its initial kinetic energy is small, and since it is only observed at high acceleration voltage. It matches D_2^+ from gas phase ionization well.

4.6. Fragmentation of clusters $D_3(-1)$ and $D_4(-1)$

The experiments here show the abundance of clusters $D_3(-1)$ and $D_4(-1)$ as scattering partners at the emitter surface, and also the corresponding ionic forms $D_3^+(1)$ and $D_4^+(1)$ in the direct laser probing of the surface layer at the emitter. Thus, it may be relevant to give some more information on these cluster forms, especially in the $D(-1)$ form. By depositing $D(-1)$ from a suitable source [10] on a metal surface, the small $D(-1)$ clusters can be observed separately from large clusters. An example of the resulting neutral TOF spectrum due to the CE in the clusters is shown in Fig. 11, using relatively low laser intensity. The results are not very sensitive to the laser parameters. The two first TOF peaks are due to D^+ ions with KER of 945 and 630 eV, from maximum-charge CE processes in clusters $D_4(-1)$ and $D_3(-1)$. (Part of the intensity in these peaks may be due to D atoms formed by electron capture by the fast D^+ in the $D(1)$ cloud). These fragmentation processes are shown with many examples also in ref. [10], thus further documentation already exists. These clusters are the basic forms also taking part in the formation of the chain clusters in $D(-1)$. Such chain clusters

are composed of D_2 and D_3 entities, further combining to D_4 and heavier fragments.

4.7. Mechanism for formation of $D(1)$ and $D(-1)$: magnetic effects

The studies presented here are a part of the ongoing work to characterize ultra-dense deuterium $D(-1)$. The relation between this material and dense deuterium $D(1)$ has been described in several publications [1,2,5,6]. The rapid inter-conversion between these two forms of material is described in the literature [7], but it is certainly not understood completely. This is however a problem of very large complexity, since $D(-1)$ is expected to be both a superfluid and a superconductor at room temperature [16,19]. This is due to the expected pairing of both deuterons and electrons. However, one interesting point for chemistry is the formation mechanism of $D(1)$ and simultaneously of $D(-1)$.

In a magnetic field, $D(-1)$ is depleted, probably due to a Meissner effect [36]. In Fig. 12, a comparison is given of the TOF results for laser fragmentation at a spot with a weak magnetic field and a spot 4 mm from that point in the same experiment in a strong magnetic field of 0.17 T. The depletion of $D(-1)$ and the strongly coupled form $D(1)$ is clearly visible in the magnetic field. Instead of falling down to these levels which cannot exist in the magnetic field, the condensed deuterium material accumulates in the $D(2)$ excitation level. This is the first positive identification of the RM level $n_B = 2$ for any atom. These results also suggest that $D(-1)$ is a superconductor at room temperature, but the fundamental understanding of such materials needs to be further developed before this can be concluded with certainty.

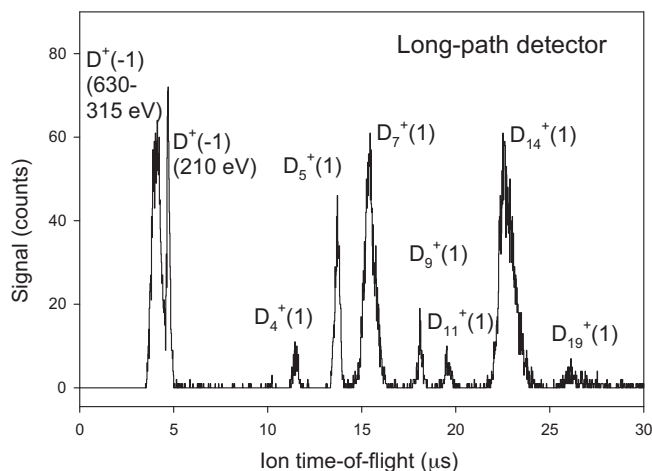


Fig. 10. Well resolved TOF-MS spectrum taken with the long-path TOF detector (112 cm). Ion peaks from both $D(-1)$ and $D(1)$ are observed, with several cluster ion peaks from $D(1)$. Emitter voltage 400 V. See Table 6 for observed and calculated TOF-MS peaks.

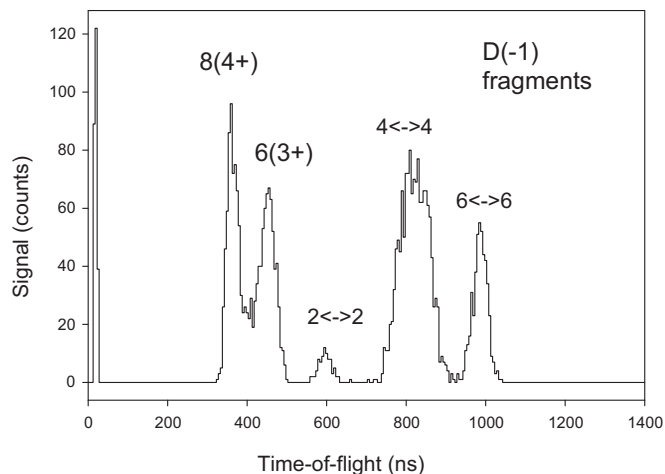


Fig. 11. TOF spectrum from $D(-1)$ clusters deposited on a metal surface. The TOFs are 340, 430, 575, 810 and 960 ns in the peaks shown. $8(4+)$ indicates the process $D_4^{4+} \rightarrow 4 D^+$, each with 945 eV KER. $6(3+)$ indicates $D_3^{3+} \rightarrow 3 D^+$, each with 630 eV KER.

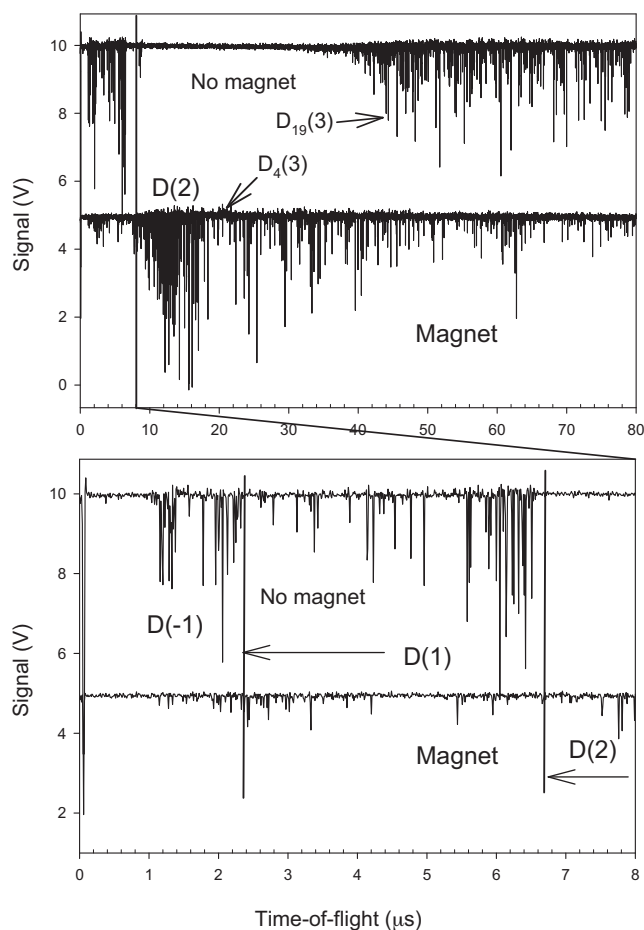


Fig. 12. TOF oscilloscope spectra from a metal surface with deposited D(-1) and higher levels D(1)–D(3), with and without a magnetic field. Single-shot spectra. The amount of D(-1) and D(1) is strongly decreased in the magnetic field, while D(2) instead becomes the lowest possible excitation level for the clusters in which the deuterium material accumulates.

5. Discussion

5.1. Dimer ions from D(-1) excluded

Most information extracted from the TOF-MS spectra with variable acceleration voltage is already described quite completely above. That the signals are due to ions and cluster ions is concluded from the direct comparison of TOF-MS spectra taken with detectors at short and long flight distances, as also done previously [2]. It is also concluded that well-defined kinetic energies are given to the ions prior to acceleration in the external field. It is further concluded that the only mechanism that can give such high, well-defined and even structured energy release is a CE process. This conclusion is based on the detailed interpretations given in the tables and also in previous publications on D(-1) [1,2,5,6,8,10]. The observed details of the CE process also make it certain that the small bond distance of 2.3 pm in D(-1) is correct, as done previously. Also the reflection of ions D^+ from clusters of the material D(-1) on the surface is concluded to be observed from the good agreement of the TOF peak positions, for example in Tables 2 and 5.

Another mechanism which would give similar TOF for the second peak in the spectra for example in Fig. 3 is that the kinetic energy for a cluster ion D_2^+ should be the same as for the ion D^+ . To be explicit, by using the ion energy of 550 eV found for the first D^+ peak at 500 V voltage in Table 2 for an ion D_2^+ , the observed TOF for the second peak of 571 ns in Fig. 3 is reproduced quite well.

Also the variation of this second peak with the acceleration voltage is given quite well by using the kinetic energy derived from the spectra for the D^+ also for an ion D_2^+ . However, this mechanism does not work for the second group of peaks in Fig. 7, where the calculated TOF values become 577, 615 and 640 ns instead of the observed values 583, 603 and 613 ns given in Table 5. Further confirming proof that this model does not match the results is found with a long flight path in Fig. 10 and Table 6. The second peak at 4.69 μ s cannot be matched by this model. This mechanism can also be rejected for theoretical reasons since it requires that the D^+ and D_2^+ ions formed should have very similar kinetic energies from the CE, despite that they would receive different kinetic energies if they were split off the same small cluster. This would imply that there is some relation between the sizes of the heavier cluster fragments for D^+ and D_2^+ ejection, or even some relation between the amount of KER transferred to rotation for these different fragments in the case of rotational KER as in Figs. 3 and 5. That the ion D_2^+ would be formed by adding an atom D to D^+ with no other change in the energetics is highly unlikely. Thus, it is concluded that a dimer ion from D(-1) is not formed and that the scattering description of the second peak in the spectra is accurate. As seen in Fig. 11, peaks for neutral dimers D_2 are observed, and this point is discussed further below. The difference between the neutral TOF and the TOF-MS experiments should be noted. In the neutral TOF experiments as in Fig. 11 a break-up of a cluster after the CE process will not be observed, since the neutral particles will move to the detector with their initial velocities given by the CE unchanged. In the TOF-MS experiments, such a break-up will give a different TOF of the lighter ion by acceleration in the applied electric field, and thus only ions stable for the entire TOF will be observed as ion peaks in the spectra.

5.2. Ion scattering process in D(-1) layer

The reflection of D^+ ions from the emitter surface will depend on the density of the material in the surface and on the collision cross section. Assuming a small cross section of 10^{-4} \AA^2 (1 pm^2) means that the mean free path will be of the order of 10^6 m at 10^{-5} mbar gas pressure, which is the maximum pressure used in the experiments. If the cross section is 1 \AA^2 , the mean free path will be 100 m in the gas in the chamber, thus still a very low probability for any kind of reflection. If the density on the emitter corresponds to that of D(1), the mean free path is still as short as 3 \mu m at the small cross section of 10^{-4} \AA^2 . For compact D(-1), the mean free path is 12 pm using this small cross section. Of course, if the mean free path is much longer than the typical interatomic distance in the material on the surface, multiple collisions will take place and the reflection efficiency may fall drastically. Thus, it can easily be concluded that no normal material will give the reflections observed, and that only the known and independently derived properties of D(-1) will make a large degree of ion reflection possible from the surface.

The next point to discuss is related to the intensity of the direct and reflected ion peaks, as seen for example in Figs. 3 and 7. In both these cases, the intensity of the two first peaks (groups of peaks) is practically the same, thus indicating the same number of ions formed by CE initially directed into and out from the surface. The factors which influence the number of reflected ions in ISS [32,37] are mainly the cross section for scattering from the surface atoms and the survival probability for the scattering ion, in this case D^+ . (Shadowing or blocking is deemed negligible in this vertical (perpendicular) impact and observation case.) The equal intensity of the two TOF peaks indicates that all D^+ ions directed into the surface layer collides with clusters D_3 or D_4 and not with any other atoms, for example in the solid emitter surface below. In general, ISS scattering is from the first few monolayers in the surface at normal material densities. The density of the surface layer

here composed of $D(-1)$ or possibly partially $D(1)$ is much larger than for any other material, as discussed above. Thus, the cross section for collisions with the topmost surface layer is large due to the high density in the surface. The survival probability for the scattered D^+ ions appears to be unity, which is an unusual case since some neutralization normally takes place. However, the electrons are strongly bound in $D(-1)$ with its bond energy of the order of 700 eV or more [16,19,34]. Since the maximum energy to gain by transferring an electron to D^+ is only 13.6 eV, this process is highly unlikely in the case of $D(-1)$, and thus the ions are not neutralized by impact on $D(-1)$. If $D(1)$ exists instead in the surface layer, the process of electron transfer to D^+ becomes more likely since the work function of $D(1)$ is of the order of a few eV [38]. Thus, charge transfer is likely in $D^+D(1)$ collisions. However, D^+ ion reflection from $D(1)$ will not work anyway. The ions will just lose their energy in collisions with D atoms since the $D(1)$ clusters will be fragmented by the impinging ion [33]. Thus, it is concluded that the surface layer probed is in the form $D(-1)$ since the scattered intensity is very high.

This size of the scattered peaks is also useful in an argument concerning the possibility of more complex mass transfer scattering processes at the surface of the type $D^+ + D_N(1) \rightarrow D_{1+n}^+ + D_{N-n}(1)$ mentioned above. Due to the weak bonding in the $D_N(1)$ clusters, they will be fragmented by the impinging D^+ ions with typically a few hundred eV of kinetic energy. Thus such a scattering process is not possible, since no heavy mass will remain intact to reflect the complex ions from the surface. If the clusters on the surface instead are $D_N(-1)$ as assumed here, they will not be fragmented. The probability of transferring several atoms of type $D(-1)$ to instead bind to the incoming D^+ ion, forming a complex ion $D_n(-1)^+$ which should then be backscattered seems small. That the ion would retain its initial kinetic energy in this process while strongly attaching to the picked-up atoms, and also avoid being scattered at large angles from the normal (perpendicular) initial direction is highly unlikely. It is concluded that the size of the slow ion peaks and the good match to the observed initial energies indicate that the interaction process at the surface is an ion scattering process as concluded above, not a complex mass transfer reaction.

5.3. Cluster forms in $D(-1)$ and $D(1)$

It can be observed directly in the experiments that the two forms $D(1)$ and $D(-1)$ are closely interrelated. For example, in an electric field the TOF-MS spectra change with a period of a few seconds from spectra with mainly $D(-1)$ peaks to mainly $D(1)$ peaks and back again [7]. The period is not independent of the laser repetition frequency, and thus a beat frequency is probably observed. It seems that the true conversion period is less than 1 s. This observation means that the bond distances of 150 pm in the material $D(1)$ [24] shrink a factor of 65 to the bond distance in $D(-1)$ which is 2.3 pm [1,2], and increase back again. It is likely that inside the emitter, this “breathing” motion is constricted by the surrounding emitter material, but on the surface of the emitter this process may take place continuously. The breathing was first observed with a large laser focus of 100 μm , but it seems to be more easily observed with a focus (beam waist) size of 4–10 μm . This indicates that there exists a certain size of the breathing domains, and that this size is larger than 4–10 μm . It is still not necessary that the domains are internally connected (bound) on this scale, only that they react for example on the motion of the electrons or ions during the conversion. Due to the superfluid and superconductive properties of $D(-1)$ [16,19] long-range interactions are expected for example in the form of Cooper pairs.

The $D(1)$ clusters will probably not be identical to the clusters of the $D(-1)$ material. In fact, clusters in $D(-1)$ are here observed

from the reflections of D^+ to mostly have a maximum size of $N=4$, while $D(1)$ gives quite well defined cluster sizes up to $N=17$ in the TOF-MS studies. This indicates that the chains of $D(1)$ may break up to smaller parts during the shrinking to $D(-1)$, probably to clusters D_4 and D_3 as observed in the experiments. Of course, when the material shrinks to $D(-1)$, some long-range coupling may still exist to other clusters and parts of the material, but the immediate surroundings in space (on the scale of the clusters) become empty. This may of course be the reason for a rapid re-expansion to $D(1)$ distances, where contact to form larger clusters like the chains in Fig. 9 can be regained. In many experiments on $D(-1)$, large clusters of the chain type are also observed. Their often symmetrical cleavage has been interpreted as due to rotational effects coupled to the vortices in the superfluid material (to be submitted).

From this description, it is apparent that larger clusters, either planar with $N=7, 19, 37, \dots$ or with close-packed closed forms with $N=6, 12, \dots$ will probably not have time to establish themselves by their usual build-up sequences [35]. These cluster series dominate in RM at excitation levels $n_B \geq 3$ (planar clusters) or $n_B = 1$ (close-packed forms). Here, another type of material is clearly observed, with another type of structure. The reason for the planar structure of RM at high excitation levels is of course the planar orbits of the Rydberg electrons. The reason for the close-packed shapes for $n_B = 1$, primarily only observed for $H(1)$, is that the form of the average electron density is neither spherical nor planar but instead more donut-shaped [4]. In the case of $D(1)$, the same form of the electron density as in $H(1)$ is expected. However, neutral TOF results support the chain cluster model for the $D(-1)$ with similar structures also for the $D(1)$ phase. This means that dimers or tetrahedrons, and trimers are the likely forms of the $D(-1)$ material at relatively low densities with a loose filamentary structure which will make the inter-conversion between $D(1)$ and $D(-1)$ possible. The studies of maximum-charge fragmentation of $D_3(-1)$ and $D_4(-1)$ clusters as in Fig. 11 support this view. The process $2 \leftrightarrow 2$ also observed in this figure is indeed the corresponding process for the cluster $D_2(-1)$.

While this discussion covers the likely forms of the neutral clusters in the surface layer on the emitter, the ionic forms also need to be described. No ions $D_N^+(-1)$ are in fact observed, but only the corresponding $D_N^+(1)$ ions with $N=3$ and 4 which dominate the spectra. This indicates that the state of $D(-1)$ requires pairing of both deuterons and electrons to exist, and that it indeed is a condensed matter state, not easily existing for a very small number of nuclei and electrons. Consider an ion $D_2^+(-1)$ with strong pairing between the deuterons, but with only one electron. Such a cluster would not be expected to exist for a long period of time. This view is in agreement with experiments since no such ions are observed. Thus the dimer ion is not stable, as was further discussed above in Section 5.1. In the case of larger clusters $D_3(-1)$ and $D_4(-1)$ the results on their fragmentation forming three or four free ions (normally converted to atoms by rapid electron transfer) described above with reference to Fig. 11 is quite clear. Such cluster ions are not stable either. Of course, they are transiently stable during the CE process. For example in Fig. 11, the correct energy from CE processes like $D_2^+ \leftrightarrow D_2^+$ is given to fragments which move correctly (as ions or neutrals) to the detector in this case with no applied electric field. With an applied field, such ions are not observed since the ions accelerated are just D^+ . Thus, the reason for the violent break-up of the various clusters $D_N(1)$ after ionization is probably the lack of stability when the correct pairing of electrons and deuterons is not possible. This is in agreement with the neutral fragmentation experiments on large $D(-1)$ clusters, as in Figs. 11 and 12. In such cases the pairing of electrons in the clusters can still exist (maybe just during the CE process as described above) which may give a larger stability. Further studies in this direction are in progress.

6. Conclusions

Clusters $D_N(-1)$ of ultra-dense deuterium have been observed by laser-induced fragmentation previously, but the direct observation of the corresponding cluster ions has not been possible, in contrast to the dense phase $D(1)$ which gives a large number of ion clusters $D_N^+(1)$ in the experiments. Here, we attempt to observe these types of ions directly by TOF-MS but no such cluster ions are observed. The $D(-1)$ clusters are formed by pairing of deuterons and electrons, giving a material which is expected to be both superfluid and superconductive. Removing an electron in such a cluster will probably destroy this special bonding. However, the experiments in another way give direct evidence for strongly bonded neutral clusters $D_N(-1)$. These clusters are observed by reflections of D^+ ions with energies below 1 keV from the ultra-dense surface layer, similar to ion surface scattering (ISS, LEIS). The clusters observed in this way in the surface layer are mainly $D_3(-1)$ and $D_4(-1)$. The ion clusters which come from the dense phase $D(1)$ and are detected by TOF-MS are mainly D_3^+ and D_4^+ . $D(1)$ and $D(-1)$ are two forms of matter which interconvert rapidly.

Acknowledgement

We thank Stephan R. Fuelling for proposing and taking part in extensive studies of magnetic field interaction with ultra-dense deuterium of which Fig. 12 is only a small part.

References

- [1] S. Badiei, P.U. Andersson, L. Holmlid, *Int. J. Hydrogen Energy* 34 (2009) 487.
- [2] S. Badiei, P.U. Andersson, L. Holmlid, *Int. J. Mass Spectrom.* 282 (2009) 70.
- [3] A. Kotarba, L. Holmlid, *Phys. Chem. Chem. Phys.* 11 (2009) 4351.
- [4] L. Holmlid, *Surf. Sci.* 602 (2008) 3381.
- [5] S. Badiei, P.U. Andersson, L. Holmlid, *Phys. Scr.* 81 (2010) 045601.
- [6] P.U. Andersson, L. Holmlid, *Phys. Lett. A* 373 (2009) 3067.
- [7] S. Badiei, P.U. Andersson, L. Holmlid, *Appl. Phys. Lett.* 96 (2010) 124103.
- [8] P.U. Andersson, L. Holmlid, *Phys. Lett. A* 374 (2010) 2856.
- [9] S. Badiei, P.U. Andersson, L. Holmlid, *Laser Part. Beams* 28 (2010) 313.
- [10] P.U. Andersson, B. Lönn, L. Holmlid, *Rev. Sci. Instrum.* 82 (2011) 013503.
- [11] É.A. Manykin, M.I. Ozhovan, P.P. Poluékto, *Sov. Phys. Tech. Lett.* 6 (1980) 95.
- [12] E.A. Manykin, M.I. Ojovan, P.P. Poluektov, *Proc. SPIE* 6181 (2006) 618105.
- [13] É.A. Manykin, M.I. Ozhovan, P.P. Poluékto, *Sov. Phys. JETP* 75 (1992) 440.
- [14] L. Holmlid, *Chem. Phys.* 237 (1998) 11.
- [15] L. Holmlid, H. Hora, G. Miley, X. Yang, *Laser Part. Beams* 27 (2009) 529.
- [16] F. Winterberg, *Phys. Lett. A* 374 (2010) 2766.
- [17] N.W. Ashcroft, *J. Low Temp. Phys.* 139 (2005) 711.
- [18] B. Militzer, R.L. Graham, *J. Phys. Chem. Solids* 67 (2006) 2136.
- [19] F. Winterberg, *J. Fusion Energy* 29 (2010) 317.
- [20] L. Holmlid, *J. Mol. Struct.* 885 (2008) 122.
- [21] J. Wang, L. Holmlid, *Chem. Phys.* 277 (2002) 201.
- [22] L. Holmlid, *Mol. Phys.* 105 (2007) 933.
- [23] S. Badiei, L. Holmlid, *J. Fusion Energy* 27 (2008) 296.
- [24] S. Badiei, L. Holmlid, *J. Phys. B: At. Mol. Opt. Phys.* 39 (2006) 4191.
- [25] S. Badiei, L. Holmlid, *Phys. Lett. A* 344 (2005) 265.
- [26] S. Badiei, L. Holmlid, *Chem. Phys.* 282 (2002) 137.
- [27] G.R. Meima, P.G. Menon, *Appl. Catal. A* 212 (2001) 239.
- [28] M. Muhler, R. Schlögl, G. Ertl, *J. Catal.* 138 (1992) 413.
- [29] L. Holmlid, *Int. J. Mass Spectrom.* 300 (2011) 50.
- [30] S. Badiei, L. Holmlid, *Mon. Not. R. Astron. Soc.* 333 (2002) 360.
- [31] L. Holmlid, *Chem. Phys.* 358 (2009) 61.
- [32] M. Aizawa, S. Lee, S.L. Anderson, *Surf. Sci.* 542 (2003) 253.
- [33] W.K. den Otter, H.H. Brongersma, H. Feil, *Surf. Sci.* 306 (1994) 215.
- [34] Andersson, P.U., Holmlid, L. submitted for publication.
- [35] L. Holmlid, *J. Cluster Sci.* 21 (2010) 637.
- [36] T. Guénault, *Basic Superfluids*, Taylor and Francis, London, England, 2003.
- [37] H. Niehus, E. Bauer, *Surf. Sci.* 47 (1975) 222.
- [38] J.P. Perdew, H.Q. Tran, E.D. Smith, *Phys. Rev. B* 42 (1990) 11627.